Effects of ultrasound, radial extracorporeal shock waves, and electrical stimulation on rat bone defect healing

Inoue, Shota ; Hatakeyama, Junpei ; Aoki, Hitoshi ; Kuroki, Hiroshi ; Niikura, Takahiro ; Oe, Keisuke ; Fukui, Tomoaki ; Kuroda, Ryosuke ;…

(Citation)
Annals of the New York Academy of Sciences,1497(1):3-14

(Issue Date)
2021-08

(Resource Type)
journal article

(Version)
Accepted Manuscript

Effects of ultrasound, radial extracorporeal shock wave, and electrical stimulation on rat bone defect healing

Short title: Effects of Physical Agents on bone defect healing

Shota Inoue [1], Junpei Hatakeyama [1], Hitoshi Aoki [2], Hiroshi Kuroki [3], Takahiro Niikura [4], Keisuke Oe [4], Tomoaki Fukui [4], Ryosuke Kuroda [4], Toshihiro Akisue [5], Hideki Moriyama [5*]

[1] Department of Rehabilitation Science, Graduate School of Health Sciences, Kobe University, Kobe, Japan

[2] OG Wellness Technologies Co., Ltd., Okayama, Japan

[3] Department of Physical Therapy, Human Health Sciences, Graduate School of Medicine, Kyoto University, Kyoto, Japan

[4] Department of Orthopaedic Surgery, Kobe University Graduate School of Medicine, Kobe, Japan

[5] Life and Medical Sciences Area, Health Sciences Discipline, Kobe University, Kobe, Japan

[*]**Correspondence:**

Hideki MORIYAMA, Ph.D.

Professor

Life and Medical Sciences Area, Health Sciences Discipline, Kobe University

Tomogaoka 7-10-2, Suma-ku, Kobe, Hyogo, 654-0142, Japan

Tel & Fax +81 78 796 4574

E-mail morihide@harbor.kobe-u.ac.jp

Abstract

Fractures associated with osteoporosis are major public health concerns. Current treatments for fractures are limited to surgery or fixation, leading to long-term bedrest which is linked to increased mortality. Alternatively, utilization of physical agents has been suggested as a promising therapeutic approach for fractures. Here, we examined the effects of ultrasound, radial extracorporeal shock waves, and electrical stimulation on normal or osteoporotic fracture healing. Femoral bone defects were created in normal or ovariectomized rats. Rats were divided into four groups: untreated, and treated with ultrasound, shock wave, or electrical stimulation after surgery. Samples were collected at 2 or 4 weeks after surgery, and the healing process was evaluated with micro-CT, histological, and immunohistochemical analyses. Ultrasound at intensities of 0.5 and 1.0 W/cm^2, but not 0.05 W/cm^2, accelerated the new bone formation. Shock wave exposure also increased the newly formed bone, but formed the abnormal periosteal callus around the defect site. Conversely, electrical stimulation did not affect the healing process. Ultrasound exposure increased osteoblast activity and cell proliferation and decreased sclerostin-positive osteocytes. We demonstrated that higher intensity ultrasound and radial extracorporeal shock wave accelerate fracture healing, but shock wave treatment may increase risk of periosteal callus formation.

Keywords Ultrasound; Radial extracorporeal shock wave; Electrical stimulation; Fracture healing

Introduction

Osteoporosis is characterized by low bone mass and poor bone microarchitecture, leading to a higher fracture susceptibility.[1] Current treatments for fractures involve surgery or fixation, resulting in prolonged bedrest; however, the long-term bedrest following fractures is linked to increased incidences of pulmonary embolism and heart failure,[2,3] and even mortality.[4] Therefore, novel treatment strategies are needed to accelerate fracture healing. We believe that one such promising treatment might be physical agents: ultrasound, radial extracorporeal shock wave, and electrical stimulation.

Among of the physical agents, low-intensity pulsed ultrasound (LIPUS) is the most widely prescribed for fracture healing.[5] However, accumulating recent evidence has shown the lack of LIPUS efficacy,[6–8] justifying the search for more effective physical agents and for optimal stimulation parameters to maximize the potential of physical agents for accelerating fracture healing.

To our current knowledge, no *in vivo* studies have investigated the biological effects of different physical agents on fracture healing. Furthermore, although it has been generally accepted that postmenopausal estrogen deficiency affects fracture healing process,[9–11] most *in vivo* studies of physical agents have focused on a single stimulation intensity or animal model.[12–22] We hypothesized that physical agents accelerate fracture healing and the responses to the physical agents can differ by its type and stimulation intensity. Hence, the present study aimed to verify the effects of three physical agents (ultrasound, radial extracorporeal shock waves, and electrical stimulation) with various intensities on fracture healing processes in normal or osteoporotic rats. The goal of our study was to develop novel and more effective therapeutic approaches for fractures utilizing physical agents, as an alternative to conventional treatments.

Materials and Methods

Experimental design and animal care

The protocols for the experiments were approved by our institutional animal care and use committee and according to the Kobe University Animal Experimentation Regulations (approval number: P160607). Male (n = 56, 5-6 months old, 500-600 g) and female (n = 36, 5-6 months old, 250-350 g) Wistar retired breeder rats were purchased from Japan SLC (Shizuoka, Japan). The animals were housed in pairs in polycarbonate cages with bedding and were maintained under artificial conditions at a constant temperature of 22 ± 1 °C with constant humidity of 55% ± 5% and a 12-hour light-dark cycle. They were allowed free access to standard food and water 24 hours a day.

We investigated the effects of the physical agents on fracture repair in two experiments (normal and osteoporotic fracture models). In the study of the normal fracture healing, male rats were anesthetized by intraperitoneal administration of 40 mg/kg sodium pentobarbital, and bone defects 1.2 mm in diameter was created in mid-diaphysis region of the bilateral femur as a reproducible and stable model of bone healing.[23–25] The defects penetrated the cortex to the medullary cavity but did not penetrate the opposite cortex. Male rats were chosen to avoid the effects of estrogen on bone turnover.[9] Then, the animals were randomly divided into four groups: untreated after the bone defect creation (BD group) and treated with ultrasound (BD + US group), radial extracorporeal shock wave (BD + rESW group), or electrical stimulation (BD + ES group) after surgery (Fig. 1A). The physical agent treatments for 1 week or 2 weeks with different stimulation intensity (0.05, 0.5, or 1.0 W/cm^2 for US group; 1, 2, or 4 bar for rESW group; 8 or 16 mA for ES group) were started one day after surgery.

In the study of the osteoporotic fracture repair, female rats received bilateral ovariectomy to simulate postmenopausal osteoporosis. After 8 weeks of ovariectomy, bone

defects 1.2 mm in diameter and 2.5 mm deep were created in the metaphysis of the bilateral femurs (about 2 mm from the growth plate) of the rats as previously described.[26,27] Then, the animals were randomly divided into four groups: untreated after the bone defect creation (OVX-BD group) and treated with ultrasound (OVX-BD + US group), radial extracorporeal shock wave (OVX-BD + rESW group), or electrical stimulation (OVX-BD + ES group) after surgery (Fig. 1B). Starting from one day after the bone defect creation, the rats were treated for 4 weeks with each physical agent with different stimulation intensity: 0.05, 0.5, or 1.0 W/cm^2 for US group; 1, 2, or 3 bar for rESW group; 8 or 16 mA for ES group.

All animals were euthanized by exsanguination under general anesthesia and analgesia at the end of the experimental period. For the BD groups, the bilateral femurs were harvested at 1 week for histological analyses (n = 3 limbs from 3 rats per group) or 2 weeks for micro-computed tomography (μCT) and histological analyses (n = 4 limbs from 4 rats per group). We used the left femurs for μCT analyses and the right femurs for histological analyses. The histological and biomechanical changes were assessed only in the BD and BD + US groups. For the OVX-BD group, the bilateral femurs were harvested at 12 weeks, and we used the left femurs for μCT and biomechanical analyses (n = 4 limbs from 4 rats per group) and the right femurs for histological analyses (n = 4 limbs from 4 rats per group).

Ultrasound

The animals received daily 20-min ultrasound exposure for 1 week or 2 weeks (BD + US group) or 4 weeks (OVX-BD + US group) after the bone defect creation. Bilateral hindlimbs of each rat were shaved and the ultrasound gel was applied. A plane circular transducer, 3.7 cm in diameter, with ultrasound device (SONICCTIZER, MINATO Medical Science Co., Ltd., Osaka, Japan) was then positioned over the experimental wound of each hindlimb, while the animals were under general anesthesia. The device work at 20% duty cycle from 1

kHz of a pulse repetition frequency and generates a sine wave at 1.0 MHz with the LIPUS intensity (spatial-averaged temporal-averaged intensity [I_{SATA}] = 0.05 W/cm^2) or the higher intensity than LIPUS which minimizes thermal effects (I_{SATA} = 0.5 or 1.0 W/cm^2). [28]

Radial extracorporeal shock wave

The rats were treated with radial extracorporeal shock wave only once (BD + rESW group) or four times of one weekly session (OVX-BD + rESW group). Both hind legs of the rats were shaved, and a 15 mm-diameter probe was used and positioned over the experimental wound of each hindlimb which applied an ultrasonic gel, while the animals were under general anesthesia. The probe was connected to the radial shock wave device (Physio-ShockMaster, SAKAI Medical Co., Ltd., Tokyo, Japan) and each femur was exposed to radial pressure waves which consisted in a total of 2,000 shock waves per one session, at 5 Hz with three different intensities of 1, 2, or 4 bar for the BD + rESW group or 1, 2, or 3 bar for the OVX-BD + rESW group.

Electrical stimulation

The rats received electrical stimulation daily for 10 min per day, for 2 weeks (BD + ES group) or 4 weeks (OVX-BD + ES group) after the bone defect creation. Both hind legs of the rats were shaved, and the rats were anesthetized. The bilateral quadriceps were then electrically stimulated by paired gold surface electrodes 7 mm in diameter. The electrodes were connected to an electrical stimulator (ASPIA TS-1000; Nihon Medix, Chiba, Japan) to transmit a square pulse at a frequency of 10 Hz and a rest-insertion period of 1 s contraction followed by 4 s rest with two different intensities of 8 or 16 mA.

Micro-computed tomography (μCT)

Cross-sectional scans were made at the drilled sites in each femur sample using micro three-dimensional (3D) X-ray CT system (R_mCT2; Rigaku, Tokyo, Japan) with an isotropic voxel resolution of 20 μm was employed at a voltage 90 kV and current 160 μA. The scanned data were reconstructed by image analysis software (TRI/3D-BON; Ratoc, Tokyo, Japan). For the quantification of the newly formed bone, the regions of interest (ROI) with a cube (750 × 750 × 750 μm^3) were placed into the central bone defect area. Thresholds value of 690 HA/mg^3 for the diaphyseal defects in the BD groups to define cortical bone[29] or 184 HA/mg^3 for the metaphyseal defects in the OVX-BD groups to define total bone including cortical and trabecular bone[30] were used to define the newly formed bone which characterized by bone volume fraction (BV/TV), trabecular number (Tb.N), trabecular thickness (Tb.Th), and trabecular separation (Tb.Sp).

Biomechanical testing

The mechanical properties of the bone defect sites were assessed by an indentation test as previously described.[31] The femurs were placed on the base fixed in a mechanical testing machine (AUTOGRAPH, Shimadzu, Kyoto, Japan). A cylindrical indenter of 1.0 mm in diameter was applied to the center of the bone defect at a constant displacement velocity of 1 mm/min. The indenter was allowed to penetrate the medullary cavity. The maximum load was obtained from the load-deflection curve and determined as the strength of the newly formed bone in the defect area. The biomechanical test in the OVX-BD + rESW group could not be carried out because of the difficulty of visual confirmation of the metaphyseal defect site due to the presence of diffuse fracture callus around the defects.

Histology

Histological preparation

Non-demineralized frozen sections were prepared according to the method described by Kawamoto.[32] Briefly, the femur was freeze-embedded with super cryoembeding medium (SCEM, Leica Microsystems, Tokyo, Japan) in isopentane at -75 °C. Cross-sections of the femur in the coronal plane (5 μm thick) were cut from each sample and were then used for histological or immunohistochemical analyses.

Histological analysis

For general histological studies, frozen sections were stained with von Kossa, safranin O/fast greens, alkaline phosphatase (ALP), or tartrate-resistant acid phosphatase (TRAP) (TRAP/ALP stain kit®; FUJIFILM Wako Pure Chemical, Tokyo, Japan), according to the manufacturers' instructions. For histomorphometric analysis of ALP and TRAP staining, two random field of view per sample were randomly taken from the bone defect regions with a light microscope (BX53; Olympus, Tokyo, Japan) and a camera (DP73; Olympus) at a magnification of 20X. Osteoblast surface was measured manually using Image J 1.50 (National Institutes of Health, Bethesda, MD, USA) as the total length of ALP-positive surface divided by bone surface. Osteoclast surface was similarly analyzed following TRAP staining.

Immunohistochemistry

Following the protocols in our laboratory,[33] the tissue sections were immunostained using against sclerostin (diluted 1:800; AF1589, R&D Systems, Minneapolis, MN, USA) or proliferating cell nuclear antigen (PCNA; 1:1500, D3H8P, Cell Signaling Technology, Danvers, MA, UA). Immunoreactivity was visualized with diaminobenzidine tetrahydrochloride reagent (ImmPACT™ DAB peroxidase substrate kit, SK-410, Vector Lab., Burlingame, CA, USA). Then, the sections were counterstained Mayer's hematoxylin

for sclerostin or hematoxylin for PCNA. The immunolabeled sections were captured with the light microscope (BX-53; Olympus) and the camera (DP73; Olympus) at a magnification of 20X. For sclerostin, the number of sclerostin-positive and total osteocytes were manually counted in two random regions of the cortical bone around the bone defect area per sample. For PCNA, the number of immune-positive cells was manually counted in one random fields of view in the bone defect regions per sample.

Statistical analysis

Statistical analyses were conducted with EZR (Saitama Medical Center, Jichi Medical University, Saitama, Japan), which is a graphical user inter face for R (The R Foundation for Statistical Computing, Vienna, Austria).[34] First, all data were checked for normality with the Shapiro-Wilk test. Normality was observed in all analyses, and the results were compared among groups with the one-way ANOVA test followed by the Tukey HSD test. All values are presented here as mean ± standard deviation (SD). *P* values less than 0.05 were considered significant. A post hoc power analysis was used to confirm that sufficient number of animals had been used.

Results

Morphologic changes in diaphyseal defect

3D reconstructions of the newly formed bone in the diaphyseal defects showed that the rats treated with ultrasound at 0.5 and 1.0 W/cm^2 had more new bone than untreated rats (Fig. 2A). This was confirmed by increased BV/TV and Tb.N in the 0.5 and 1.0 W/cm^2 US-treated groups compared to the BD group ($P < 0.05$, power = 1.00) (Fig. 2B and Supplementary Table 1). Furthermore, representative histological evidence of bone mineralization supported the findings obtained by μCT analysis (Fig. 2C). The newly formed

bone across the cortical gap was thicker and denser in the 0.5 and 1.0 W/cm^2 US-treated groups compared to the untreated group.

Morphologic changes in metaphyseal defect

Representative images in the femoral metaphyseal defect sites revealed that the defects in the OVX-BD + US and rESW groups, except for the US group at 0.05 W/cm^2, were filled with the newly formed bone compared to the OVX-BD group (Fig. 3A). Von Kossa staining showed that these groups had the more abundant bone in the defect sites than the OVX-BD group (Fig. 3B). Quantitative measurements of the newly formed bone with μCT analyses revealed that BV/TV increased in the rats treated with ultrasound at 1.0 W/cm^2 or extracorporeal shock wave at 1, 2, and 3 bar when compared to the untreated rats ($P < 0.05$, power = 1.00) (Fig. 3C). Furthermore, in the 1.0 W/cm^2 US-treated group, BV/TV was larger than in the 0.05 W/cm^2 US-treated group ($P < 0.05$). These findings were reinforced by the other structural parameters by μCT analyses (Supplementary Table 2). On the other hand, in the rats that received radial extracorporeal shock wave, the periosteal callus was observed near the defect site in the 3D images by μCT (Fig. 3A), histological sections (Fig. 3B and 3D, left), and macroscopic observation (Fig. 3D, right).

Biomechanical properties

The biomechanical strength of the new bone in the defect sites which was determined by the maximum load showed no differences between the untreated and treated groups both in the normal and osteoporotic rats.

Osteoblast and osteoclast activity

In the diaphyseal defects, ALP-positive regions increased in the 0.5 and 1.0 W/cm^2 US-treated groups compared to the untreated ($P < 0.05$, power = 0.96) (Fig. 4A, top and B). TRAP staining revealed the localization of osteoclast in the diaphyseal defects at 7 days after surgery (Fig. 4A, bottom). There was no significant change in the percentage of osteoclast surface among all groups (power = 0.95) (Fig. 4C).

In the metaphyseal defects, ALP-stained bone surfaces in the OVX-BD + rESW and US at 1.0 W/cm^2 were higher than OVX-BD group ($P < 0.05$, power = 1.00) (Fig. 5A and B). TRAP-positive regions were observed in all groups (Fig. 5C), but there were no significant differences in the percentage of osteoclast surface among all groups (power = 1.00) (Fig. 5D).

Immunohistochemical pattern of sclerostin and PCNA

The sclerostin-positive osteocytes around the defect area were tended to decreased in the 1.0 W/cm^2 US-treated group (versus untreated, $P = 0.09$, power = 0.96) (Fig. 6A, top and Table 2). In the metaphyseal defects, the percentage of sclerostin-positive osteocytes decreased in the OVX-BD + US at 1.0 W/cm^2 and rESW groups when compared to the OVX-BD group ($P < 0.05$, power = 1.00).

In the BD + US at 0.5 and 1.0 W/cm^2 groups, PCNA-positive cells were densely distributed in the bone marrow at the defect area when compared to the untreated group at 7 days after the surgery (Fig. 6, bottom). The number of PCNA-positive cells increased in the 0.5 and 1.0 W/cm^2 US-treated group ($P < 0.05$, power = 0.97) (Table 2).

Discussion

This study investigated the effects of ultrasound, radial extracorporeal shock wave, and electrical stimulation on normal or osteoporotic fracture healing in rat bone defect models.

As a result, ultrasound at higher intensity (0.5 and 1.0 W/cm^2) accelerated normal fracture healing, but not radial extracorporeal shock wave and electrical stimulation. We found that high intensity ultrasound exposure increased cell proliferation and osteoblast activity at the healing site. The results in the osteoporotic fracture model showed that ultrasound at higher intensity (1.0 W/cm^2) and radial extracorporeal shock wave accelerate fracture healing under estrogen-deficient conditions. However, we also found that shock wave treatment may increase risk of the abnormal periosteal callus formation.

Based on the μCT analyses, ultrasound at intensity 0.05 W/cm^2 did not affect the new bone formation in the bone defect both in the normal and osteoporotic rats. This accords with previous clinical[7,8] and animal reports,[35–37] showing no stimulatory effect of LIPUS at intensity less than 0.1 W/cm^2 on fracture healing processes. Meanwhile, ultrasound at higher intensity (0.5 or 1.0 W/cm^2) than LIPUS accelerated bone formation at the bone defect site both in the normal and osteoporotic rats. These are similar to the report that ultrasound at intensity 0.3 W/cm^2 accelerated bone formation in the bone defect, but not at intensity 0.1 W/cm^2.[35] Moreover, ultrasound exposure at various intensities ranging from 0.015 to 0.15 W/cm^2 [38] or 0.005 to 0.1 W/cm^2 [39] improved estrogen-deficient bone loss in an intensity-dependent manner. In line with these previous findings, our results indicate that ultrasound exposure at higher intensity than LIPUS enhances bone formation both in normal and osteoporotic fracture healing. Although high intensity ultrasound can induce some side effects such as skin necrosis at 2.5 W/cm^2 [40] and osteonecrosis with increased bone resorption at 2.2 W/cm^2 [41], the rats treated with ultrasound at 0.5 and 1.0 W/cm^2 had no gross, physical, or histological abnormalities. Consequently, these findings suggest the possibility that higher intensity ultrasound than LIPUS is a promising noninvasive treatment for fracture healing.

Consistent with previous reports showing the effectiveness of focused extracorporeal shock wave in fracture healing,[15,16,42,43] radial extracorporeal shock wave increased the newly formed bone in the osteoporotic fracture model. Furthermore, the shock wave at all three intensities (1, 2, and 3 bar) increased the newly formed bone, indicating that this treatment can accelerate osteoporotic fracture healing, irrespective of the stimulation intensity. Although radial shock waves have the advantage of being lower energy and less pain for patients than focused shock waves, in this study, its exposure also induced the diffuse callus formation around the bone defect. In the metaphyseal defect model, a small amount of the periosteal callus is observed during the healing process, and its formation peaks at day 14 and is completely resorbed at day 28 to 35 after the defect creation.[44] Meanwhile, the callus induced by the shock wave still remained in the defect site at 4 weeks after surgery and was greater than that of the untreated rats, implying the abnormal bone healing process. Taken together, these findings indicate that radial extracorporeal shock wave in one weekly session accelerate osteoporotic fracture healing, but its treatment may potentially increase the abnormal callus formation.

Ultrasound and radial extracorporeal shock wave accelerated fracture healing, while muscle contraction induced by electrical stimulation did not affect the new bone formation in both normal and osteoporotic fractures. This is inconsistent with a previous animal study showing that the electrically-induced muscular contraction enhances fracture healing in rabbits.[22] Although the defect area is filled with the hematoma and fibrous tissue rapidly after surgery,[24] the bone defect may be less likely to respond to longitudinal stress induced by muscular contraction than the transverse fracture. Thus, muscle contraction induced by electrical stimulation may be insufficient to affect bone defect healing.

We evaluated the mechanical strength of the newly formed bone at the defect sites using the indentation test, which has been widely used in measuring the biomechanical

properties of bone in different experimental conditions.[31] As a consequence, ultrasound exposure at higher intensity had no effect on maximum load in normal and osteoporotic rats, despite increased new bone mass at the defect site. The bone strength is determined not only by the quantity of bone tissue but also by its quality, which is characterized by the trabecular microarchitecture, the mineral and collagen, and the shape of bones.[45] Whether ultrasound exposure affects the bone quality is unclear in this study, but our results indicate that its exposure for 2 or 4 weeks does not affect the bone strength at the healing site.

Bone defect healing occurs mainly through intramembranous ossification via direct differentiation of osteoblasts from mesenchymal cells in the initial phase of the healing process.[24] Ultrasound at 0.5 and 1.0 W/cm^2 increased ALP activity, a differentiation marker of osteoblasts,[46] in the normal fracture model at the initial phase of defect healing (7 days after surgery). In the osteoporotic rats, ultrasound at 1.0 W/cm^2 and radial extracorporeal shock waves at 1 and 3 bar also enhanced its activity at the later phase (4 weeks after surgery), implying that these treatments could activate osteoblasts both in the initial and later phases of healing processes. In addition, high intensity ultrasound and shock wave were tended to decrease sclerostin-positive osteocytes, paralleled by increased osteoblast activity. Sclerostin inhibits the osteoblast differentiation and activity by antagonizing Wnt/β catenin signaling.[47] Additionally, sclerostin deficient mice enhances intramembranous ossification of bone defects by increasing the β-catenin expression and osteoblast number.[48] Thus, these findings suggest that higher intensity ultrasound and radial extracorporeal shock wave activate osteoblasts, at least in part, via downregulation of sclerostin in osteocytes, thereby accelerating bone healing.

Cell proliferation is essential for fracture healing processes, particularly in the early stages of the healing.[49,50] Consistent with the previous reports,[14,51–53] ultrasound at intensity 0.05 W/cm^2 did not affect the number of PCNA-positive cells, a marker of cell

proliferation[54], at the early phase of defect healing (7 days after surgery). In contrast, ultrasound at 0.5 and 1.0 W/cm^2 enhanced cell proliferation at the same time point, as indicated by increased PCNA-positive cells at the bone defect site. This corresponds to the report that high magnitude strain in the physiological range stimulates cell proliferation of bone marrow stromal cells.[55] Collectively, these findings suggest that higher intensity ultrasound enhanced cell proliferation, in addition to osteoblast differentiation, leading to accelerated fracture healing.

This study had several limitations. The differences in sex, age, and the defect site make it difficult to compare the results between normal and osteoporotic rats. Therefore, we cannot conclude from the present study whether the response of physical agents differed with or without estrogen. In addition, we could not examine the effects of physical agents on endochondral ossification. The bone defect model has been used in many studies of fracture healing as a reproducible and stable model.[23–27] This model is healed only by intramembranous ossification,[56] while transverse fracture healing in humans occurs through not only intramembranous but also endochondral ossification.[57] Our study showed that the physical agents enhanced intramembranous ossification, but their stimulatory effect on endochondral ossification cannot at present be answered. Therefore, further research should explore the safety and efficacy of physical agents in clinical trials and animal studies with transverse fractures.

In conclusion, we demonstrated that higher intensity ultrasound than LIPUS accelerates both normal and osteoporotic fracture healing. Our findings also showed that radial extracorporeal shock wave enhances osteoporotic fracture healing, but its treatment may increase risk of the abnormal periosteal callus formation. Future studies are needed to determine if our findings are clinically applicable.

Acknowledgments

This work was supported by the Japan Society for the Promotion of Science KAKENHI Grant No. 16K12933 and Suzuken Memorial Foundation. We thank Mr. Masato Nomura, Mr. Yoshio Wakimoto, Mr. Ryota Suzuki, Mr. Takumi Yakuwa, Mr. Changxin Li, Mr. Taisei Wakigawa, Mr. Toshiya Tsubaki, and Ms. Sae Kinoshita for their skilled technical assistance; Asst. Prof. Akira Ito and Dr. Akihiro Nakahata for their support with mechanical testing; and Asst. Prof. Noriaki Maeshige for support with the ultrasound transducer. We are also grateful to SAKAI Medical Co., Ltd. for providing the radial extracorporeal shock wave device; and Nihon Medix Co., Ltd. for providing the electrical stimulator.

Competing interests

The authors declare no competing interests.

Reference

1. NIH Consensus Development Panel on Osteoporosis Prevention, Diagnosis. and Therapy 2001. Osteoporosis prevention, diagnosis, and therapy. *JAMA* **285**: 785–795.
2. Wehren L.E., W.G. Hawkes, D.L. Orwig, *et al.* 2003. Gender Differences in Mortality after Hip Fracture: The Role of Infection. *J. Bone Miner. Res.* **18**: 2231–2237.
3. Roche J.J.W., R.T. Wenn, O. Sahota, *et al.* 2005. Effect of comorbidities and postoperative complications on mortality after hip fracture in elderly people: Prospective observational cohort study. *Br. Med. J.* **331**: 1374–1376.
4. Vestergaard P., L. Rejnmark & L. Mosekilde. 2007. Increased mortality in patients with a hip fracture-effect of pre-morbid conditions and post-fracture complications. *Osteoporos. Int.* **18**: 1583–1593.
5. Watanabe Y., T. Matsushita, M. Bhandari, *et al.* 2010. Ultrasound for Fracture Healing: Current Evidence. *J. Orthop. Trauma* **24**: S56–S61.
6. Lou S., H. Lv, Z. Li, *et al.* 2018. Effect of low-intensity pulsed ultrasound on distraction osteogenesis: A systematic review and meta-analysis of randomized controlled trials. *J. Orthop. Surg. Res.* **13**: 1–10.
7. Busse J.W., M. Bhandari, T.A. Einhorn, *et al.* 2016. Re-evaluation of low intensity pulsed ultrasound in treatment of tibial fractures (TRUST): Randomized clinical trial. *BMJ* **355**: i5351.
8. Schandelmaier S., A. Kaushal, L. Lytvyn, *et al.* 2017. Low intensity pulsed ultrasound for bone healing: systematic review of randomized controlled trials. *BMJ* **356**: j656.
9. McCann R.M., G. Colleary, C. Geddis, *et al.* 2008. Effect of osteoporosis on bone mineral density and fracture repair in a rat femoral fracture model. *J. Orthop. Res.* **26**: 384–393.

10. Namkung-Matthai H., R. Appleyard, J. Jansen, *et al.* 2001. Osteoporosis influences the early period of fracture healing in a rat osteoporotic model. *Bone* **28**: 80–86.

11. Lill C.A., J. Hesseln, U. Schlegel, *et al.* 2003. Biomechanical evaluation of healing in a non-critical defect in a large animal model of osteoporosis. *J. Orthop. Res.* **21**: 836–842.

12. Azuma Y., M. Ito, Y. Harada, *et al.* 2001. Low-intensity pulsed ultrasound accelerates rat femoral fracture healing by acting on the various cellular reactions in the fracture callus. *J. Bone Miner. Res.* **16**: 671–680.

13. Cheung W.-H., W.-C. Chin, L. Qin, *et al.* 2012. Low intensity pulsed ultrasound enhances fracture healing in both ovariectomy-induced osteoporotic and age-matched normal bones. *J. Orthop. Res.* **30**: 129–136.

14. Gebauer G.P., S.S. Lin, H.A. Beam, *et al.* 2002. Low-intensity pulsed ultrasound increases the fracture callus strength in diabetic BB Wistar rats but does not affect cellular proliferation. *J. Orthop. Res.* **20**: 587–592.

15. Wang C.J., K.D. Yang, F.S. Wang, *et al.* 2004. Shock wave treatment shows dose-dependent enhancement of bone mass and bone strength after fracture of the femur. *Bone* **34**: 225–230.

16. Chen X.F., H.M. Huang, X.L. Li, *et al.* 2015. Slightly focused high-energy shockwave therapy: a potential adjuvant treatment for osteoporotic fracture. *Int. J. Clin. Exp. Med.* **8**: 5044–54.

17. van der Jagt O.P., T.M. Piscaer, W. Schaden, *et al.* 2011. Unfocused Extracorporeal Shock Waves Induce Anabolic Effects in Rat Bone. *J. Bone Jt. Surgery-American Vol.* **93**: 38–48.

18. Van Der Jagt O.P., J.C. Van Der Linden, W. Schaden, *et al.* 2009. Unfocused extracorporeal shock wave therapy as potential treatment for osteoporosis. *J. Orthop. Res.* **27**: 1528–1533.

19. Van Der Jagt O.P., J.H. Waarsing, N. Kops, *et al.* 2013. Unfocused extracorporeal shock waves induce anabolic effects in osteoporotic rats. *J. Orthop. Res.* **31**: 768–775.

20. Özkan E., M.C. Bereket, M.E. Önger, *et al.* 2018. The effect of unfocused extracorporeal shock wave therapy on bone defect healing in diabetics. *J. Craniofac. Surg.* **29**: 1081–1086.

21. Koolen M.K.E., B. Pouran, F.C. Öner, *et al.* 2018. Unfocused shockwaves for osteoinduction in bone substitutes in rat cortical bone defects. *PLoS One* **13**: e0200020.

22. Park S.H. & M. Silva. 2004. Neuromuscular electrical stimulation enhances fracture healing: Results of an animal model. *J. Orthop. Res.* **22**: 382–387.

23. Chen Y.J., Y.R. Kuo, K.D. Yang, *et al.* 2004. Activation of extracellular signal-regulated kinase (ERK) and p38 kinase in shock wave-promoted bone formation of segmental defect in rats. *Bone* **34**: 466–477.

24. Chiba S., K. Okada, K. Lee, *et al.* 2001. Molecular Analysis of Defect Healing in Rat Diaphyseal Bone. *J. Vet. Med. Sci.* **63**: 603–608.

25. Kim J.B., P. Leucht, K. Lam, *et al.* 2007. Bone regeneration is regulated by Wnt signaling. *J. Bone Miner. Res.* **22**: 1913–1923.

26. Cheng N., J. Dai, X. Cheng, *et al.* 2013. Porous CaP/silk composite scaffolds to repair femur defects in an osteoporotic model. *J. Mater. Sci. Mater. Med.* **24**: 1963–1975.

27. Zhang Y., N. Cheng, R. Miron, *et al.* 2012. Delivery of PDGF-B and BMP-7 by mesoporous bioglass/silk fibrin scaffolds for the repair of osteoporotic defects. *Biomaterials* **33**: 6698–6708.

28. Baker K.G., V.J. Robertson & F.A. Duck. 2001. A Review of Therapeutic Ultrasound: Biophysical Effects. *Phys. Ther*. **81**: 1351–1358.

29. Tanaka M., A. Sakai, S. Uchida, *et al.* 2004. Prostaglandin E2 receptor (EP4) selective agonist (ONO-4819.CD) accelerates bone repair of femoral cortex after drill-hole injury associated with local upregulation of bone turnover in mature rats. *Bone* **34**: 940–948.

30. Wei L., J. Ke, I. Prasadam, *et al.* 2014. A comparative study of Sr-incorporated mesoporous bioactive glass scaffolds for regeneration of osteopenic bone defects. *Osteoporos. Int.* **25**: 2089–2096.

31. Fangel R., P. Sérgio Bossini, A. Cláudia Renno, *et al.* 2011. Low-level laser therapy, at 60 J/cm2 associated with a Biosilicate® increase in bone deposition and indentation biomechanical properties of callus in osteopenic rats. *J. Biomed. Opt.* **16**: 078001.

32. Kawamoto T. 2003. Use of a new adhesive film for the preparation of multi-purpose fresh-frozen sections from hard tissues, whole-animals, insects and plants. *Arch. Histol. Cytol.* **66**: 123–43.

33. Moriyama H., N. Kanemura, I. Brouns, *et al.* 2012. Effects of aging and exercise training on the histological and mechanical properties of articular structures in knee joints of male rat. *Biogerontology* **13**: 369–381.

34. Kanda Y. 2013. Investigation of the freely available easy-to-use software “EZR” for medical statistics. *Bone Marrow Transplant.* **48**: 452–8.

35. Lavandier B., A. Gleizal & J.C. Béra. 2009. Experimental Assessment of Calvarial Bone Defect Re-Ossification Stimulation Using Low-Intensity Pulsed Ultrasound. *Ultrasound Med. Biol.* **35**: 585–594.

36. Lirani-Galvão A.P., V. Jorgetti & O. Lopes Da Silva. 2006. Comparative study of how low-level laser therapy and low-intensity pulsed ultrasound affect bone repair in rats. *Photomed. Laser Surg.* **24**: 735–740.

37. Fávaro-Pípi E., S.M. Feitosa, D.A. Ribeiro, *et al.* 2010. Comparative study of the effects of low-intensity pulsed ultrasound and low-level laser therapy on bone defects in tibias of rats. *Lasers Med. Sci.* **25**: 727–732.

38. Sun S., L. Sun, Y. Kang, *et al.* 2020. Therapeutic Effects of Low-Intensity Pulsed Ultrasound on Osteoporosis in Ovariectomized Rats: Intensity-Dependent Study. *Ultrasound Med. Biol.* **46**: 108–121.

39. Ferreri S.L., R. Talish, T. Trandafir, *et al.* 2011. Mitigation of bone loss with ultrasound induced dynamic mechanical signals in an OVX induced rat model of osteopenia. *Bone* **48**: 1095–1102.

40. Boucaud A., J. Montharu, L. Machet, *et al.* 2001. Clinical, histologic, and electron microscopy study of skin exposed to low-frequency ultrasound. *Anat. Rec.* **264**: 114–119.

41. Lyon R., X.C. Liu & J. Meier. 2003. The effects of therapeutic vs. high-intensity ultrasound on the rabbit growth plate. *J. Orthop. Res.* **21**: 865–871.

42. Rompe J.D., T. Rosendahl, C. Schöllner, *et al.* 2001. High-energy extracorporeal shock wave treatment of nonunions. *Clin. Orthop. Relat. Res.* 102–111.

43. Kieves N.R., C.S. Mackay, K. Adducci, *et al.* 2015. High energy focused shock wave therapy accelerates bone healing: A blinded, prospective, randomized canine clinical trial. *Vet. Comp. Orthop. Traumatol.* **28**: 425–432.

44. Inoue S., H. Otsuka, J. Takito, *et al.* 2018. Decisive differences in the bone repair processes of the metaphysis and diaphysis in young mice. *Bone Reports* **8**: 1–8.

45. Viguet-Carrin S., P. Garnero & P.D. Delmas. 2006. The role of collagen in bone strength. *Osteoporos. Int.* **17**: 319–336.

46. Rawadi G., B. Vayssière, F. Dunn, *et al.* 2003. BMP-2 Controls Alkaline Phosphatase Expression and Osteoblast Mineralization by a Wnt Autocrine Loop. *J. Bone Miner. Res.* **18**: 1842–1853.

47. Sapir-Koren R. & G. Livshits. 2014. Osteocyte control of bone remodeling: is sclerostin a key molecular coordinator of the balanced bone resorption–formation cycles? *Osteoporos. Int.* **25**: 2685–2700.

48. McGee-Lawrence M.E., Z.C. Ryan, L.R. Carpio, *et al.* 2013. Sclerostin deficient mice rapidly heal bone defects by activating β-catenin and increasing intramembranous ossification. *Biochem. Biophys. Res. Commun.* **441**: 886–890.

49. Li G., G. White, C. Connolly, *et al.* 2002. Cell Proliferation and Apoptosis During Fracture Healing. *J. Bone Miner. Res.* **17**: 791–799.

50. Gerstenfeld L.C., D.M. Cullinane, G.L. Barnes, *et al.* 2003. Fracture healing as a post-natal developmental process: Molecular, spatial, and temporal aspects of its regulation. *J. Cell. Biochem.* **88**: 873–884.

51. Schumann D., R. Kujat, J. Zellner, *et al.* 2006. Treatment of human mesenchymal stem cells with pulsed low intensity ultrasound enhances the chondrogenic phenotype in vitro. *Biorheology* **43**: 431–443.

52. Lee S.Y., A. Koh, T. Niikura, *et al.* 2013. Low-Intensity Pulsed Ultrasound Enhances BMP-7-Induced Osteogenic Differentiation of Human Fracture Hematoma-Derived Progenitor Cells In Vitro. *J. Orthop. Trauma.* **27**: 29–33.

53. Kang K.S., S.J. Lee, H. Lee, *et al.* 2011. Effects of combined mechanical stimulation on the proliferation and differentiation of pre-osteoblasts. *Exp. Mol. Med.* **43**: 367–373.

54. Muskhelishvili L., J.R. Latendresse, R.L. Kodell, *et al.* 2003. Evaluation of Cell Proliferation in Rat Tissues with BrdU, PCNA, Ki-67(MIB-5) Immunohistochemistry and in Situ Hybridization for Histone mRNA. *J. Histochem. Cytochem.* **51**: 1681–1688.

55. Koike M., H. Shimokawa, Z. Kanno, *et al.* 2005. Effects of mechanical strain on proliferation and differentiation of bone marrow stromal cell line ST2. *J. Bone Miner. Metab.* **23**: 219–225.

56. Monfoulet L., B. Rabier, O. Chassande, *et al.* 2010. Drilled hole defects in mouse femur as models of intramembranous cortical and cancellous bone regeneration. *Calcif. Tissue. Int.* **86**: 72–81.

57. Einhorn T.A. 2005. The science of fracture healing. *J. Orthop. Trauma.* **19**: 19–21.

Figure legends

Fig. 1 (**A**) A Diagram of the experimental design for the studies of the normal fracture healing is shown. The bilateral femurs were harvested at 1 week for histological analyses (n = 3 limbs from 3 rats per group) or 2 weeks for μCT and histological analyses (n = 4 limbs from 4 rats per group) and biomechanical testing (n = 4 limbs from 2 rats per group). We used the right femurs for μCT analyses and the left femurs for histological analyses. (**B**) A Diagram of the experimental design for the studies of the osteoporotic fracture healing is shown. The bilateral femurs were harvested at 12 weeks, and we used the left femurs for μCT and biomechanical analyses (n = 4 limbs from 4 rats per group) and the right femurs for histological analyses (n = 4 limbs from 4 rats per group). OVX = ovariectomy; BD = bone defect; US = ultrasound; rESW = radial extracorporeal shock wave; ES = electrical stimulation

Fig. 2 Morphologic changes in the diaphyseal defect of normal rats after 2 weeks of the defect creation. (**A**) Representative 3D images show the newly formed bone at the diaphyseal defect site obtained by μCT analysis. Scale bar = 500 μm. (**B**) The graph shows quantification of the bone volume in the defect by μCT analysis (n = 4 femurs per group). Data are expressed as mean ± SD. **P* < 0.05 vs. BD group; †*P* < 0.10 vs. BD + US at 0.05 W/cm^2 group. (**C**) Representative histological images in the defect area stained with von Kossa are shown. Scale bars = 500 μm. BD = bone defect; US = ultrasound; rESW = radial extracorporeal shock wave; ES = electrical stimulation; BV/TV = bone volume/tissue volume

Fig. 3 Morphologic changes in the metaphyseal defect of osteoporotic rats after 4 weeks of the defect creation. (**A**) Representative 3D images show the metaphyseal defect site obtained

by μCT analysis. Scale bar = 2 mm. (**B**) Representative histological images in the defect stained with von Kossa are shown. Scale bars = 500 μm. (**C**) The graph shows quantification of the bone volume in the defect by μCT analysis (n = 4 femurs per group). Data are expressed as mean ± SD. **P* < 0.05 vs. OVX-BD group; †*P* < 0.05 vs. OVX-BD + US at 0.05 W/cm^2 group. (**D**) Representative histological images in the distal femur stained with safranin O/fast green (left) and macroscopic observations of the femur (right) are shown. Arrowheads indicate the site of the defect creation. Scale bars = 1 mm (left) and 5 mm (right). OVX = ovariectomy; BD = bone defect; US = ultrasound; rESW = radial extracorporeal shock wave; ES = electrical stimulation; BV/TV = bone volume/tissue volume

Fig. 4 (**A**) Representative histological images in the diaphyseal defect sites of normal rats after 1 week of the defect creation stained with ALP (top) and TRAP (bottom) are shown. Scale bars = 100 μm. (**B**) The graphs show quantification of ALP staining by osteoblast surface per bone surface (**C**) and TRAP staining by osteoclast surface per bone surface (n = 3 femurs per group). Data are expressed as mean ± SD. **P* < 0.05 vs. BD group. BD = bone defect; US = ultrasound

Fig. 5 (**A**) Representative histological images in the metaphyseal defect sites of osteoporotic rats after 4 weeks of the defect creation stained with ALP are shown. Scale bars = 100 μm. (**B**) The graph shows quantification of ALP staining by osteoblast surface per bone surface (n = 4 femurs per group). (**C**) Representative histological images in the metaphyseal defect sites stained with TRAP are shown. Scale bars = 100 μm. (**D**) The graph shows quantification of TRAP staining by osteoclast surface per bone surface (n = 4 femurs per group). Data are expressed as mean ± SD. **P* < 0.05 vs. OVX-BD group; †*P* < 0.05 vs.

561 OVX-BD + US at 0.05 W/cm^2 group; ‡$P < 0.05$ vs. OVX-BD + US at 0.5 W/cm^2 group.
562 OVX = ovariectomy; BD = bone defect; US = ultrasound; rESW = radial extracorporeal
563 shock wave; ES = electrical stimulation
564
565 **Fig. 6** Representative photomicrographs show the distribution of sclerostin in the cortical
566 bone around the diaphyseal defect area of normal rats after 2 weeks of the defect creation
567 (top). Representative photomicrographs show the distribution of PCNA in the diaphyseal
568 bone defect sites of normal rats after 1 week of the defect creation (bottom). Scale bars =
569 100 μm. BD = bone defect; US = ultrasound

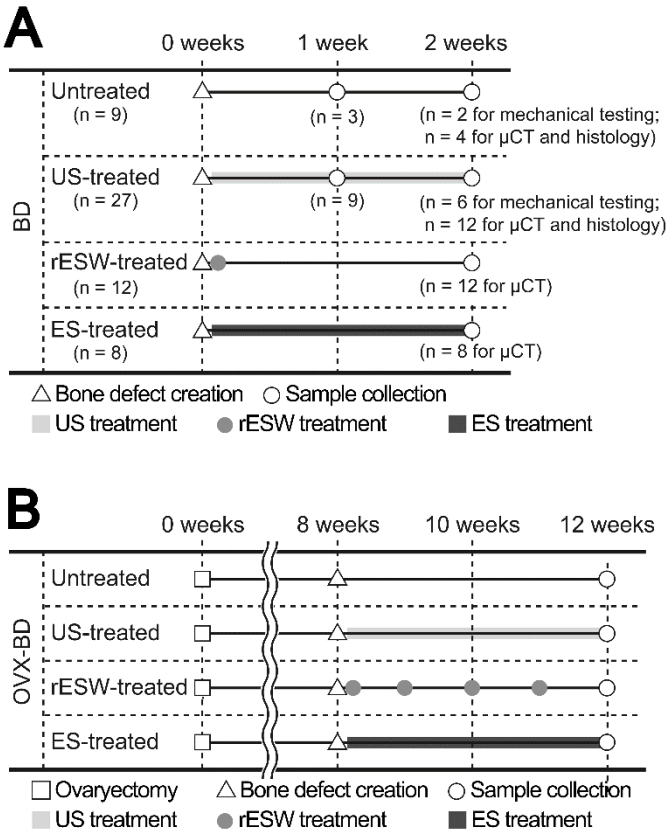
A
0 weeks
1 week
2 weeks
BD
Untreated
(n = 9)
(n = 3)
(n = 2 for mechanical testing;
n = 4 for μCT and histology)
US-treated
(n = 27)
(n = 9)
(n = 6 for mechanical testing;
n = 12 for μCT and histology)
rESW-treated
(n = 12)
(n = 12 for μCT)
ES-treated
(n = 8)
(n = 8 for μCT)
Bone defect creation
Sample collection
US treatment
rESW treatment
ES treatment
B
0 weeks
8 weeks
10 weeks
12 weeks
OVX-BD
Untreated
US-treated
rESW-treated
ES-treated
Ovaryectomy
Bone defect creation
Sample collection
US treatment
rESW treatment
ES treatment

Figure 1

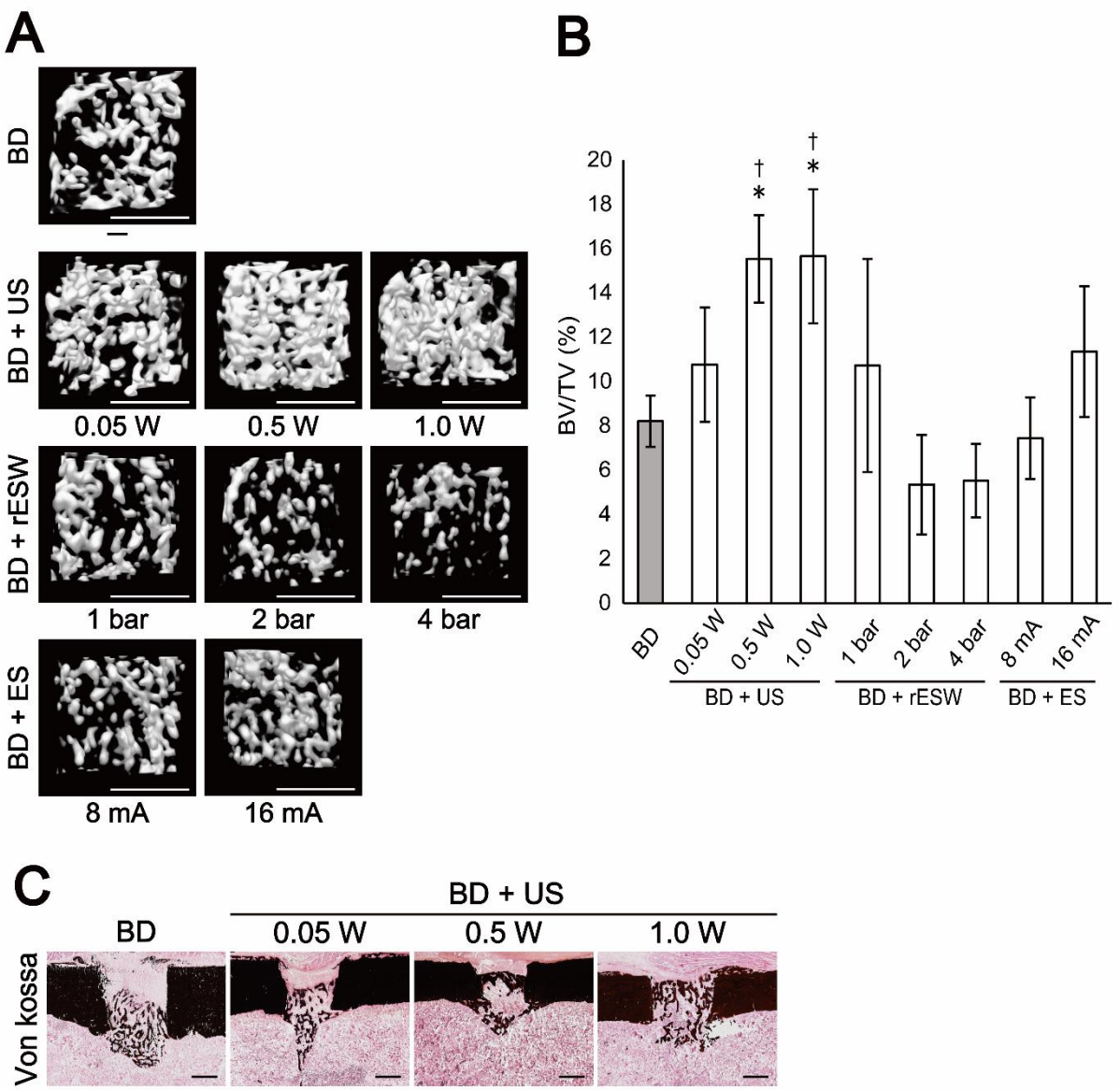
A
BD
BD + US
0.05 W
0.5 W
1.0 W
BD + rESW
1 bar
2 bar
4 bar
BD + ES
8 mA
16 mA
B
BV/TV (%)
20
18
16
14
12
10
8
6
4
2
0
BD
0.05 W
0.5 W
1.0 W
1 bar
2 bar
4 bar
8 mA
16 mA
BD + US
BD + rESW
BD + ES
C
BD + US
BD
0.05 W
0.5 W
1.0 W
Von kossa

Figure 2

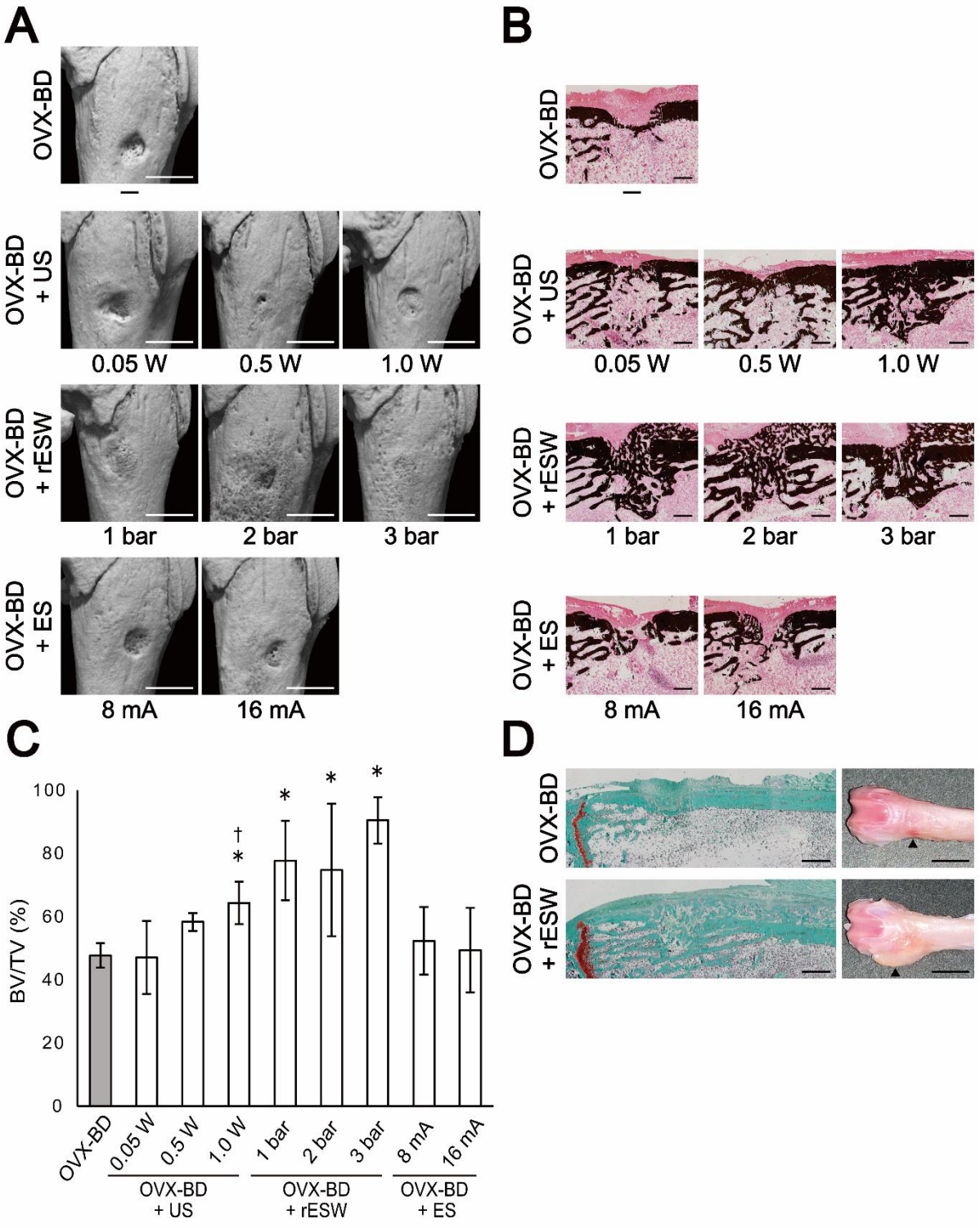
A
OVX-BD
OVX-BD + US
0.05 W
0.5 W
1.0 W
OVX-BD + rESW
1 bar
2 bar
3 bar
OVX-BD + ES
8 mA
16 mA
B
OVX-BD
OVX-BD + US
0.05 W
0.5 W
1.0 W
OVX-BD + rESW
1 bar
2 bar
3 bar
OVX-BD + ES
8 mA
16 mA
C
BV/TV (%)
100
80
60
40
20
0
OVX-BD
0.05 W
0.5 W
1.0 W
1 bar
2 bar
3 bar
8 mA
16 mA
OVX-BD + US
OVX-BD + rESW
OVX-BD + ES
D
OVX-BD
OVX-BD + rESW

Figure 3

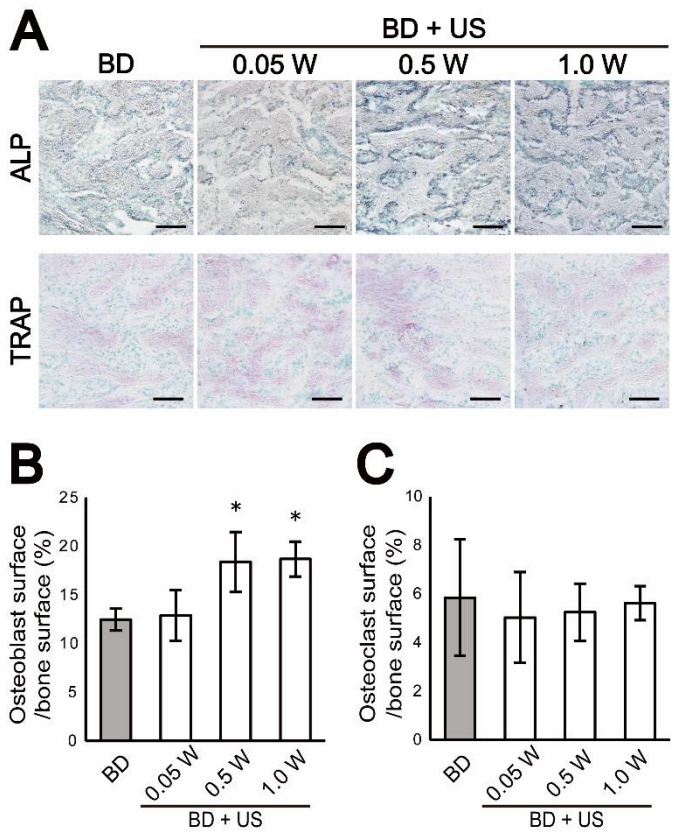
A
BD
BD + US
0.05 W
0.5 W
1.0 W
ALP
TRAP
B
Osteoblast surface /bone surface (%)
25
20
15
10
5
0
*
*
BD
0.05 W
0.5 W
1.0 W
BD + US
C
Osteoclast surface /bone surface (%)
10
8
6
4
2
0
BD
0.05 W
0.5 W
1.0 W
BD + US

Figure 4

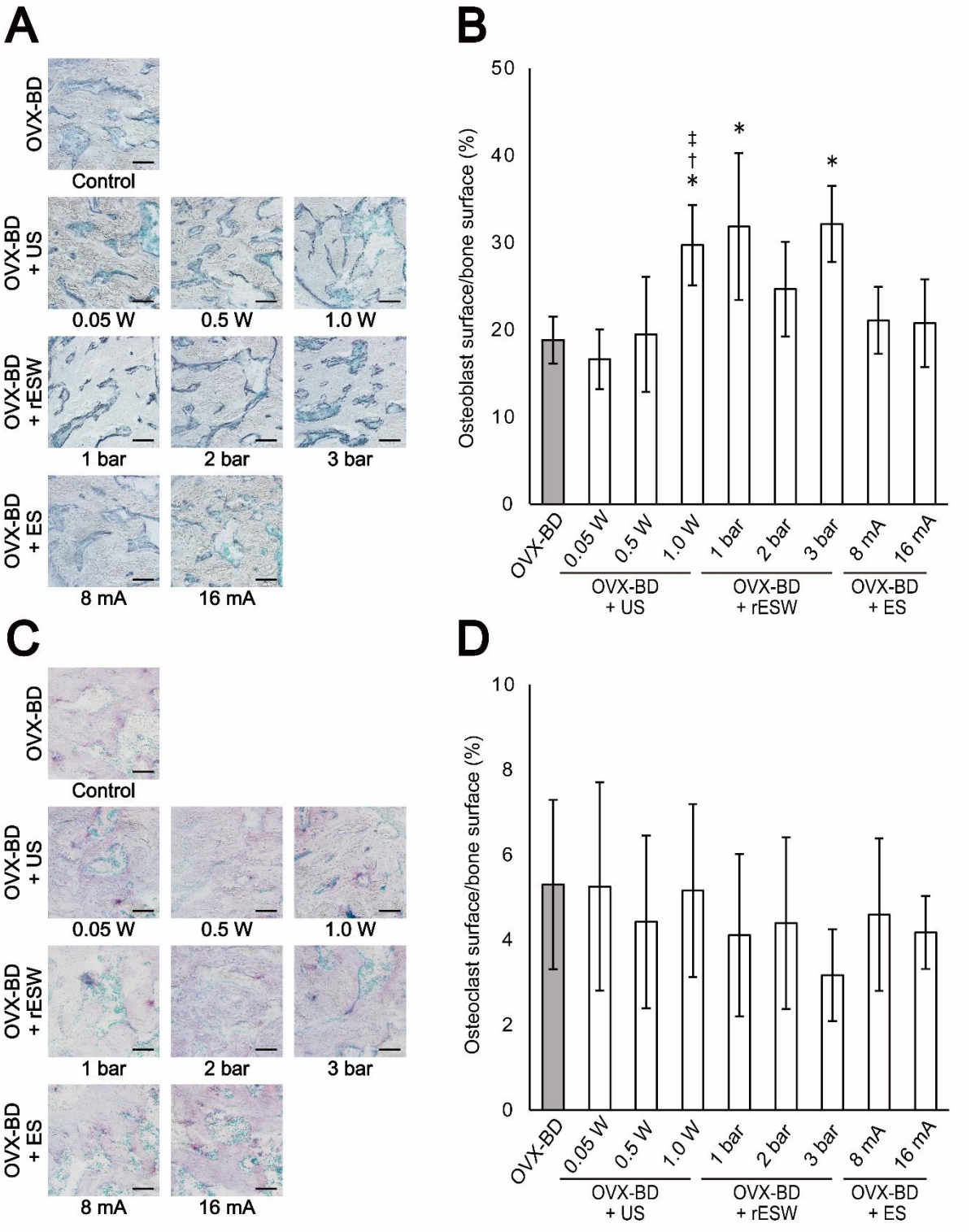
A
OVX-BD
Control
OVX-BD + US
0.05 W
0.5 W
1.0 W
OVX-BD + rESW
1 bar
2 bar
3 bar
OVX-BD + ES
8 mA
16 mA
B
Osteoblast surface/bone surface (%)
50
40
30
20
10
0
* ‡ † *
*
*
OVX-BD
0.05 W
0.5 W
1.0 W
1 bar
2 bar
3 bar
8 mA
16 mA
OVX-BD + US
OVX-BD + rESW
OVX-BD + ES
C
OVX-BD
Control
OVX-BD + US
0.05 W
0.5 W
1.0 W
OVX-BD + rESW
1 bar
2 bar
3 bar
OVX-BD + ES
8 mA
16 mA
D
Osteoclast surface/bone surface (%)
10
8
6
4
2
0
OVX-BD
0.05 W
0.5 W
1.0 W
1 bar
2 bar
3 bar
8 mA
16 mA
OVX-BD + US
OVX-BD + rESW
OVX-BD + ES

Figure 5

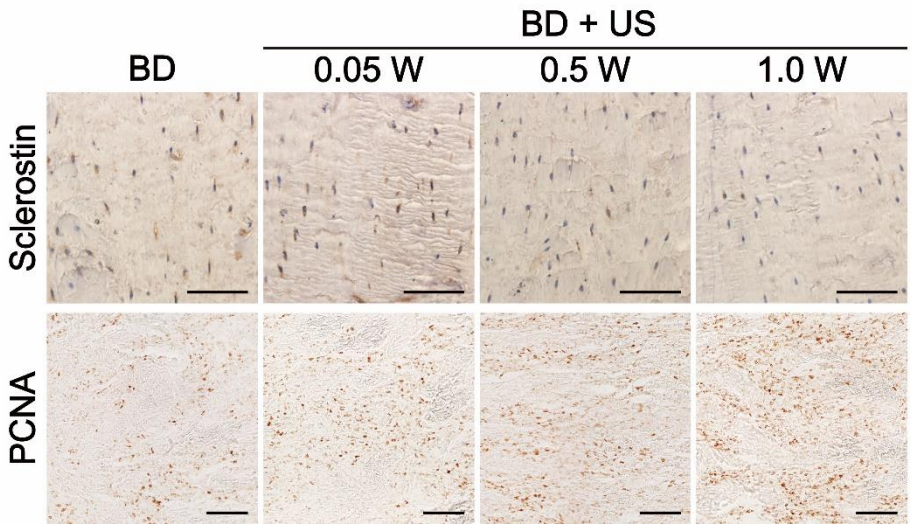

Figure 6

Table 1. Maximum load of newly formed bone in defect sites determined by mechanical testing.

Group	BD	BD + US			OVX-BD	OVX-BD + US			OVX-BD + rESW			OVX-BD + ES	
		0.05 W/cm^2	0.5 W/cm^2	1.0 W/cm^2		0.05 W/cm^2	0.5 W/cm^2	1.0 W/cm^2	1 bar	2 bar	3 bar	8 mA	16mA
Maximum load (N)	20.7 ± 5.4	34.9 ± 8.9	27.6 ± 15.0	33.2 ± 7.5	34.0 ± 6.3	31.1 ± 12.0	40.8 ± 9.2	45.2 ± 9.6	—	—	—	29.1 ± 10.6	25.2 ± 10.5

Data are expressed as mean ± SD. OVX = ovariectomy; BD = bone defect; US = ultrasound; rESW = radial extracorporeal shock wave; ES = electrical stimulation

Table 2. Quantification of immunohistochemistry for sclerostin and PCNA.

Group	BD	BD + US			OVX-BD	OVX-BD + US			OVX-BD + rESW			OVX-BD + ES	
		0.05 W/cm^2	0.5 W/cm^2	1.0 W/cm^2		0.05 W/cm^2	0.5 W/cm^2	1.0 W/cm^2	1 bar	2 bar	3 bar	8 mA	16mA
Sclerostin-positive osteocytes (%)	74.2 ± 10.6	68.8 ± 9.5	54.2 ± 19.0	47.1 ± 3.9**	60.4 ± 7.8	52.3 ± 11.6	41.7 ± 10.0	37.4 ± 6.8†	40.7 ± 12.5†	36.8 ± 4.8†	40.2 ± 11.8†	50.2 ± 12.6	48.9 ± 7.1
PCNA-positive cells (/10^5 μm^2)	17.4 ± 4.1	23.9 ± 5.7	40.2 ± 10.4*	40.6 ± 2.7*	—	—	—	—	—	—	—	—	—

Data are expressed as mean ± SD. *P < 0.05 vs. BD group; **P < 0.10 vs. BD group; †P < 0.05 vs. OVX-BD group. OVX = ovariectomy; BD = bone defect;

US = ultrasound; rESW = radial extracorporeal shock wave; ES = electrical stimulation

Supplementary Table 1. Trabecular microarchitecture of the diaphyseal defect in normal rats quantified by μCT.

Group	BD	BD + US			BD + rESW			BD + ES	
		0.05 W/cm^2	0.5 W/cm^2	1.0 W/cm^2	1 bar	2 bar	4 bar	8 mA	16 mA
Tb.N (1/μm)	1.2 ± 0.4	1.7 ± 0.2	2.0 ± 0.4*	1.8 ± 0.2	1.4 ± 0.7	1.0 ± 0.3	1.1 ± 0.3	1.5 ± 0.4	1.8 ± 0.3
Tb.Th (μm)	126.0 ± 46.9	103.8 ± 9.6	100.1 ± 22.2	84.6 ± 15.2	108.2 ± 28.9	121.1 ± 20.8	137.2 ± 9.5	109.4 ± 14.8	101.6 ± 4.0
Tb.Sp (μm)	46.9 ± 1.5	47.8 ± 3.2	50.7 ± 5.3	51.2 ± 4.2	45.9 ± 6.8	45.4 ± 2.1	44.1 ± 3.8	42.2 ± 0.3	45.4 ± 3.6

Data are expressed as mean ± SD. *P < 0.05 vs. BD group. BD = bone defect; US = ultrasound; rESW = radial extracorporeal shock wave; ES = electrical stimulation; Tb.N = trabecular bone number; Tb.Th = trabecular bone thickness; Tb.Sp = trabecular bone separation

Supplementary Table 2. Trabecular microarchitecture of the metaphyseal defect in osteoporotic rats quantified by µCT.

Group	OVX-BD	OVX-BD + US			OVX-BD + rESW			OVX-BD + ES	
		0.05 W/cm^2	0.5 W/cm^2	1.0 W/cm^2	1 bar	2 bar	3 bar	8 mA	16 mA
Tb.N (1/µm)	3.5 ± 0.3	3.4 ± 0.3	4.7 ± 0.6*†	4.4 ± 0.5*†	4.0 ± 0.2	4.4 ± 0.6*	4.2 ± 0.5	4.5 ± 1.0	4.1 ± 0.8
Tb.Th (µm)	126.7 ± 9.2	141.1 ± 35.6	125.9 ± 8.0	137.6 ± 14.8	196.1 ± 34.5*	170.3 ± 45.7	215.5 ± 18.2*	117.1 ± 19.2	125.0 ± 45.4
Tb.Sp (µm)	142.3 ± 21.1	159.1 ± 37.7	95.7 ± 26.6	108.4 ± 51.4	55.9 ± 31.3*	60.3 ± 52.7*	23.7 ± 20.0*	112.2 ± 44.6	125.9 ± 41.9

Data are expressed as mean ± SD. *P < 0.05 vs. OVX-BD group; †P < 0.05 vs. OVX-BD + US at 0.05 W/cm^2 group. OVX = ovariectomy; BD = bone defect; US = ultrasound; rESW = radial extracorporeal shock wave; ES = electrical stimulation; Tb.N = trabecular bone number; Tb.Th = trabecular bone thickness; Tb.Sp = trabecular bone separation